

# The singular perturbation of surface tension in Hele-Shaw flows

By HECTOR D. CENICEROS AND THOMAS Y. HOU

Applied Mathematics, California Institute of Technology, Pasadena, CA 91125, USA

(Received 4 April 1999 and in revised form 15 September 1999)

Morphological instabilities are common to pattern formation problems such as the non-equilibrium growth of crystals and directional solidification. Very small perturbations caused by noise originate convoluted interfacial patterns when surface tension is small. The generic mechanisms in the formation of these complex patterns are present in the simpler problem of a Hele-Shaw interface. Amid this extreme noise sensitivity, what is then the role played by small surface tension in the dynamic formation and selection of these patterns? What is the asymptotic behaviour of the interface in the limit as surface tension tends to zero? The ill-posedness of the zero-surface-tension problem and the singular nature of surface tension pose challenging difficulties in the investigation of these questions. Here, we design a novel numerical method that greatly reduces the impact of noise, and allows us to accurately capture and identify the singular contributions of extremely small surface tensions. The numerical method combines the use of a compact interface parametrization, a rescaling of the governing equations, and very high precision. Our numerical results demonstrate clearly that the zero-surface-tension limit is indeed singular. The impact of a surface-tension-induced complex singularity is revealed in detail. The singular effects of surface tension are first felt at the tip of the interface and subsequently spread around it. The numerical simulations also indicate that surface tension defines a length scale in the fingers developing in a later stage of the interface evolution.

---

## 1. Introduction

Surface tension is known to play an important role in pattern formation problems such as dendritic crystal growth and directional solidification. Dendrites are common to the micro-structural development in casting processes of metals and in needle crystals. The understanding of these structures is crucial to the design of controlling mechanisms for such technologically important processes. The generic features of the morphological instabilities encountered in these pattern formation problems are present in the relatively simple model of Hele-Shaw flows. In a Hele-Shaw cell, two incompressible fluids of different viscosities are confined between closely spaced glass plates. The problem of interest here is when the less viscous fluid displaces the more viscous fluid. The intense study of the interface motion in a Hele-Shaw cell has also been motivated by the analogy to oil displacement in a porous medium.

Significant progress has been achieved in understanding steady states and their linear stability (see e.g. the review by Pelcé 1988). However, as demonstrated by experiments (Maxworthy 1987; Arneodo *et al.* 1989), the Hele-Shaw interface does not evolve into a steady shape when the dimensionless surface tension coefficient  $B$  (defined in §2) is sufficiently small. Even very small perturbations caused by noise can

quickly grow and trigger tip-splitting processes and the formation of a convoluted (even fractal) pattern on the Hele-Shaw interface. This extreme noise sensitivity is due to the ill-posedness of the zero-surface-tension problem. The Hele-Shaw front is subject to the Mullins–Sekerka instability found in non-equilibrium crystal growth.

What is then the role played by small surface tension in the dynamic formation and selection of these complex patterns? What is the asymptotic behaviour of the interface in the limit as  $B$  tends to zero? Here, we investigate numerically these questions. Using a compact interface parametrization and rescaling of the governing equations, we derive an effective numerical method that greatly reduces the impact of noise, and allows us to capture and identify the singular contributions of extremely small values of  $B$ .

There are challenging difficulties associated with the numerical computation of the interface evolution. As in the experiments, numerical solutions experience a great sensitivity to noise when  $B$  is small. For a channel flow, DeGregoria & Schwartz (1986) and Meiburg & Homsy (1988) found that the amplitude of the perturbations causing tip-splitting decreases rapidly as  $B$  is reduced. Moreover, as shown by Bensimon (1986), and by Dai & Shelley (1993), the numerical solutions for small values of  $B$  are extremely sensitive to the round-off level noise. The growth of noise, which is essentially governed by the linearized equation of motion, is much faster than the growth of the numerical solution governed by the full nonlinear equation. Consequently, noise can quickly grow to affect significantly the interface. Numerical filtering is inefficient once the noise has grown to a relatively high level.

Investigating the limit as  $B$  tends to zero requires a perturbation analysis. More precisely, it requires understanding in what sense the small but non-zero  $B$  solutions should be compared with the corresponding zero-surface-tension solution. Mathematically, this means choosing the appropriate space and norm. For example, in any Sobolev norm defined on the interface, we may conclude that the limit as  $B$  tends to zero is regular as long as the zero-surface-tension curvature is smooth and bounded. However, due to the ill-posedness of the zero-surface-tension problem, there is no reason to expect that a small perturbation caused by the non-zero  $B$  will remain small and smooth. The perturbation analysis should be performed in a space in which the zero-surface-tension problem is well-posed. This is the space of complex analytic functions. In this space, it is possible to obtain critical information about the motion of complex singularities that may affect the physical interface.

Another difficulty is a surface-tension-induced singularity in the complex domain. Tanveer (1993) and Siegel, Tanveer & Dai (1996) have developed a remarkable asymptotic theory aimed at understanding the evolution of Hele-Shaw flows with small  $B$ . The interface motion is described by a time-dependent conformal map  $z(\zeta, t)$  that takes the interior of a unit circle in the  $\zeta$ -plane onto the physical domain of the viscous fluid in the  $z$ -plane (the displacing fluid is assumed inviscid). The unit circle itself is mapped to the free boundary. As pointed out by Tanveer (1993) a zero in  $z_\zeta(\zeta, 0)$ , with  $|\zeta| > 1$ , spawns a singularity in the  $\zeta$ -plane through the surface-tension term. This so called daughter singularity, initially coinciding with the zero of  $z_\zeta$ , moves away fast and approaches the unit circle when the zero is still far from it. If nonlinear effects are neglected this complex singularity (according to the asymptotic theory it is actually a cluster of singularities) could hit the physical domain at a time  $t_d$  when the  $B = 0$  solution is perfectly smooth. Some numerical evidence of the effects of the daughter singularity and of the singular nature of surface tension was provided by Siegel *et al.* (1996) who also confirmed some of the scalings predicted by the asymptotic theory. However, they found that it is very difficult to compute for

$B < 10^{-5}$ , even if quadruple (128-bit) precision is used. To study the limit as  $B$  tends to zero we need to separate noise from surface tension and to capture the daughter singularity for extremely small values of  $B$ . Note that the daughter singularity is created at  $t = 0+$  in the complex  $\zeta$ -plane outside the unit disk but the interface itself is analytic and its Fourier modes decay exponentially. For times of  $O(\Delta t)$ , where  $\Delta t$  is the timestep, the amplitude of the daughter singularity ( $B$  times the function  $A_d(t)$  in (3.6)) is  $O(B\Delta t)$ . Thus, many digits are required to capture information about this very weak initial singularity.

Here, we develop a novel numerical method to overcome the difficulties mentioned above. One important observation is that the effect of noise can be significantly reduced by using a parametrization that yields a compact representation of the solution in Fourier space. Out of many choices (Lagrangian, equal-arclength, etc.), the conformal map representation gives the most compact parametrization of the interface. This was first discussed by Dai & Shelley (1993). The conformal parametrization was also employed by Siegel *et al.* (1996) for its especial compact representation property. With this parametrization, we can use effectively Krasny filtering (Krasny 1986) to separate noise from the physical solution for the majority of high to intermediate modes. Moreover, based on symmetry, the structure of the conformal map in Fourier space is known (see Dai, Kadanoff & Zhou 1991) so that additional selective filtering can be used. To resolve the initially weak daughter singularity in  $|\zeta| > 1$ , we reformulate the interface evolution equation in terms of the difference between non-zero- and zero-surface-tension solutions scaled by  $B$ . This scaling allows us to effectively compute the limit as  $B$  tends to zero. The scaled equation is solved using a highly accurate time-space discretization with multiple-precision arithmetic of up to 80 digits. This high precision is needed both to capture the singular contributions of surface tension and to reduce further the effects of noise.

Our numerical results clearly identify the singular effects of surface tension on the evolution of the Hele-Shaw interface. Through a series of computations decreasing  $B$  to  $10^{-9}$  the influence of the daughter singularity is observed around the time  $t_d$  predicted by the asymptotic theory. Near that time, the absolute value of the difference between the first derivative of the zero and the non-zero- $B$  solutions does not decrease as  $B$  is reduced. Instead, the deviation from the  $B = 0$  solution grows and becomes more localized as  $B$  is decreased for a fixed time. The non-zero- $B$  curvature and its derivative deviate greatly from the corresponding  $B = 0$  quantities. For a fixed time after  $t_d$ , a pronounced increase in the deviation of these quantities and a shrinkage of the length scale are observed as  $B$  is reduced. On the other hand, for a fixed  $B$ , our numerical experiments show in detail how an extremely small but non-zero- $B$  solution is affected in time by the presence of the daughter singularity. The singular effects are first felt (before  $t_d$ ) at the tip of the interface and subsequently spread around it. The spreading in time of the affected region supports the theory that the daughter singularity is actually a cluster of singularities. The numerical simulations also indicate that surface tension defines a length scale in the fingers developing in a later stage of the interface evolution.

A more mathematical question is that of the all-time existence of solutions for any surface tension. Duchon & Robert (1984) have shown the local-in-time existence of smooth solutions for initial data that correspond to a graph of a sufficiently smooth function. There is also a global-in-time existence result by Constantin & Pugh (1993) for initial data close to a circle and without pumping. But, to our knowledge, there is no proof of existence of *analytic* solutions, even for a short time, for *general* analytic initial data. At a later stage our computations detect an abrupt and large growth

of the curvature in time for a fixed but very small  $B$  ( $10^{-8}$ ). This rapid variation of curvature detected by the numerics can give the impression of a finite-time curvature singularity. However a more plausible explanation of this behaviour is provided by the asymptotic theory. The daughter singularity cluster will asymptotically shrink to a point, in the limit as  $B$  is decreased. The compact cluster will get within a maximal distance of  $O(B^{1/2})$  to the unit disk but will not hit it in finite time. Since  $z_{\zeta\zeta}$  scales as  $B^{-1/3}$  in the inner region characterizing the daughter singularity cluster, the impact of this cluster on the physical domain can cause curvature to change from  $O(1)$  to  $O(B^{-1/3})$  over an  $O(B^{1/3})$  time scale. The rescaling features of the asymptotic theory inner-scale equation (Siegel *et al.* 1996) suggest that, if solutions exist for larger  $B$ , they will exist for any non-zero  $B$ , at least well beyond  $t_d$ . If this is the case, surface tension will define a length scale according to the minimum distance of the complex singularity to the unit disk.

The rest of the paper is organized as follows. In §2, the governing equations for the Hele-Shaw interface are presented. In §3, we describe briefly how the curvature-induced complex singularity is generated. We devote §4 to describe the numerical method. In §5, we present numerical results for both fixed time (past  $t_d$ ) and decreasing  $B$ , and longer time behaviour for fixed  $B$ . Further discussion of the results and conclusions are given in §6.

## 2. The equations of motion

We consider a bubble of inviscid fluid penetrating into a viscous incompressible fluid in a Hele-Shaw cell. There is a source at the origin pumping mass at a constant rate. The viscous fluid outside the bubble has a velocity field  $\mathbf{u}$  given by Darcy's law

$$\mathbf{u} = -\frac{b^2}{12\mu}\nabla p, \quad (2.1)$$

where  $\mu$  is the viscosity,  $p$  is the pressure, and  $b$  is the spacing between the two plates in the Hele-Shaw cell. The incompressibility and Darcy's law imply that the pressure satisfies the Laplace equation

$$\nabla^2 p = 0. \quad (2.2)$$

Here, we represent the interface motion by a time-dependent conformal map  $z(\zeta, t)$  that takes the interior of the unit circle in the  $\zeta$ -plane onto the physical domain of the viscous fluid in the  $z$ -plane. The unit circle itself is mapped to the Hele-Shaw interface. Because of the presence of the source at the origin,  $z$  has the following form:

$$z(\zeta, t) = \frac{a(t)}{\zeta} + f(\zeta, t), \quad (2.3)$$

where  $f$  is an analytic function inside the disk, and  $a(t)$  is real and positive. The kinematic condition states that the motion of the interface in the normal direction is given by the normal component of the fluid velocity. Thus,

$$\operatorname{Re} \left\{ \frac{z_t}{\zeta z_\zeta} - \frac{\zeta \Phi_\zeta}{|z_\zeta|^2} \right\} = 0 \quad \text{on } |\zeta| = 1, \quad (2.4)$$

where  $\Phi$  is a complex velocity potential.

Surface tension introduces a jump in the pressure proportional to the local curvature  $\mathcal{K}$ . Since the pressure inside the bubble is constant, we can write the dynamic

boundary condition as follows:

$$\operatorname{Re}\{\Phi\} = \frac{B}{|z_\zeta|} \operatorname{Re}\left[1 + \zeta \frac{z_{\zeta\zeta}}{z_\zeta}\right] \quad \text{on } |\zeta| = 1, \tag{2.5}$$

where  $B = 2\pi b^2 T / (12\mu Q a(0))$  is a dimensionless surface tension parameter. Here  $T$  is the surface tension and  $Q$  is the injection rate. We non-dimensionalize all variables by taking  $Q = 2\pi$  and  $a(0) = 1$ . Letting  $Z(\alpha, t) = z(e^{i\alpha}, t)$ , using the boundary conditions (2.4) and (2.5), and well-known relations between the real and imaginary parts of an analytic function on the unit circle, we obtain the following evolution equation (for a derivation see for example Constantin & Kadanoff 1991):

$$Z_t = F(Z_\alpha) + BG(Z_\alpha), \tag{2.6}$$

where

$$F(Z_\alpha) = -iZ_\alpha(I - iH)|Z_\alpha|^{-2}, \tag{2.7}$$

and

$$G(Z_\alpha) = iZ_\alpha(I - iH)[|Z_\alpha|^{-2}H\mathcal{K}_\alpha]. \tag{2.8}$$

Here  $\mathcal{K}$  is the mean curvature which, after setting  $Z = X + iY$ , is given by

$$\mathcal{K} = \frac{Y_{\alpha\alpha}X_\alpha - X_{\alpha\alpha}Y_\alpha}{(X_\alpha^2 + Y_\alpha^2)^{3/2}}. \tag{2.9}$$

The subscript  $\alpha$  means differentiation with respect to that variable.  $H$  is the periodic Hilbert transform defined as

$$Hf(\alpha) = \frac{1}{2\pi} \text{PV} \int_0^{2\pi} \cot \frac{1}{2}(\alpha - \alpha') f(\alpha') d\alpha'. \tag{2.10}$$

There are several classes of exact  $B = 0$  solutions (Saffman 1959; Howison 1986*a, b, c*; Shraiman & Bensimon 1984). In particular, we are interested in comparing non-zero- $B$  solutions with those zero-surface-tension solutions for which  $z_\zeta(\zeta, 0)$  has at least one zero for  $|\zeta| > 1$ . As we will see in the next section, in the presence of surface tension, each zero of  $z_\zeta(\zeta, 0)$  spawns a complex (daughter) singularity through the curvature. For concreteness, we consider the following expanding bubble with three-fold symmetry (see Shraiman & Bensimon 1984):

$$z(\zeta, t) = \frac{A(t)}{\zeta} \left[1 + \frac{\zeta^3}{2\zeta_0^3(t)}\right], \tag{2.11}$$

where

$$A(t) = A(0)\zeta_0^3(0) \left[1 - \left(1 - \frac{2}{\zeta_0^6(0)} + \frac{1}{\zeta_0^{12}(0)} - \frac{4t}{\zeta_0^6(0)A^2(0)}\right)^{1/2}\right]^{1/2}, \tag{2.12}$$

and

$$\zeta_0(t) = \zeta_0(0) \left(\frac{A(0)}{A(t)}\right)^{1/3}. \tag{2.13}$$

The parameters  $A(0)$  and  $\zeta_0(0)$  are real numbers satisfying  $A(0) > 0$  and  $|\zeta_0(0)| > 1$ . Here, we take  $A(0) = 1$  and  $\zeta_0(0) = 1.2$ . The derivative  $z_\zeta$  has three zeros located at  $\zeta = \zeta_0(t)$ ,  $\zeta = \zeta_0(t)e^{2\pi i/3}$ , and  $\zeta = \zeta_0(t)e^{4\pi i/3}$ . These zeros approach the unit disk and

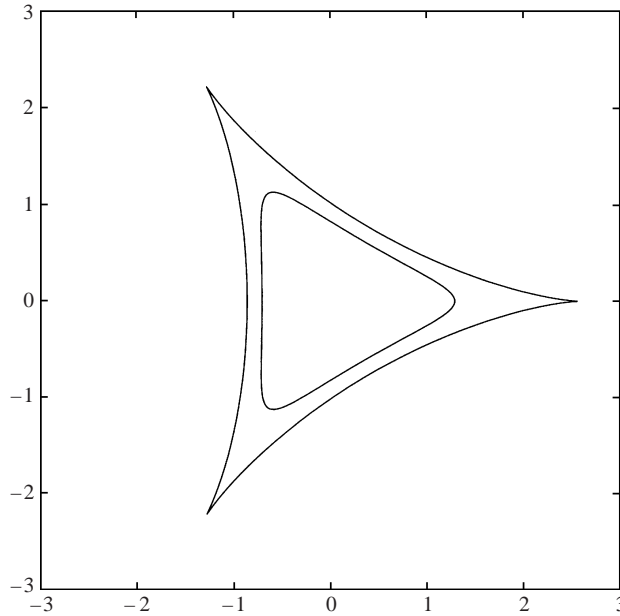


FIGURE 1. Exact zero-surface-tension solution for  $\zeta_0(0) = 1.2$  at  $t = 0$  and  $t_c = 0.3302$ .

impinge on it at a time  $t_c$  ( $\zeta_0(t_c) = 1$ ) given by

$$t_c = \left[ \frac{A(0)(\zeta_0^6(0) - 1)}{2\zeta_0^3(0)} \right]^2. \tag{2.14}$$

At this time  $t_c$ , the solution has three singularities in the form of cusps. For  $A(0) = 1$  and  $\zeta_0(0) = 1.2$ ,  $t_c = 0.3301$ . Figure 1 shows the zero-surface-tension exact solution both at  $t = 0$  and  $t = t_c$ .

### 3. The daughter singularity

Here, we describe briefly how an initial zero in  $z_\zeta(\zeta, 0)$  introduces a complex singularity through the curvature when  $B > 0$ . We refer the reader to Tanveer's original work (Tanveer 1993) and also to Siegel *et al.* (1996) for the details and the complete description of the asymptotic theory.

The perturbation analysis requires extending the equations of motion to  $|\zeta| > 1$ . First, equation (2.6) can be analytically continued into the domain  $|\zeta| < 1$  by the use of the Poisson integral formula. The analytic continuation to  $|\zeta| > 1$  is achieved by contour deformation.

In the domain  $|\zeta| > 1$ , the extended evolution equation has the following form:

$$z_t = q_1 z_\zeta + q_2 + B(q_3(z_\zeta)_{\zeta\zeta}^{-1/2} + r), \tag{3.1}$$

where  $q_1$ ,  $q_2$ , and  $q_3$  are analytic functions of  $\zeta$  in  $|\zeta| > 1$ . The function  $r$  contains surface tension terms which are less singular than  $(z_\zeta)_{\zeta\zeta}^{-1/2}$  in the neighbourhood of a zero of  $z_\zeta(\zeta, 0)$ . The explicit forms of these functions are irrelevant to this discussion.

The well-posedness of the zero-surface-tension problem in the extended complex domain  $|\zeta| > 1$  allows a perturbation expansion for small  $B$  of the form

$$z(\zeta, t) = z_0(\zeta, t) + Bz_1(\zeta, t) + \dots, \tag{3.2}$$

where  $z_0$  is the zero-surface-tension solution (see Tanveer 1993). Then  $z_0$  and  $z_1$  satisfy the following equations:

$$z_{0t} = q_{10}z_{0\zeta} + q_{20}, \tag{3.3}$$

$$z_{1t} = q_{10}z_{1\zeta} + q_{30}(z_{0\zeta})_{\zeta\zeta}^{-1/2} + \dots, \tag{3.4}$$

where the subscript 0 on any  $q_i$  term denotes its evaluation using the corresponding  $B = 0$  solution.

The most surprising and interesting result obtained by the formal asymptotics is when  $z_\zeta(\zeta, 0)$  contains a zero. Let

$$z_\zeta(\zeta, 0) \sim D(0)(\zeta - \zeta_0(0)) \quad \text{for } |\zeta_0(0)| > 1, \tag{3.5}$$

then in order to balance the most singular term  $(z_{0\zeta})_{\zeta\zeta}^{-1/2}$  in the curvature, for short times and in a neighbourhood of  $\zeta_0$ ,  $z_1$  has to have the following form:

$$z_1 \sim A_0(t)(\zeta - \zeta_0(t))^{-3/2} + A_d(t)(\zeta - \zeta_d(t))^{-3/2} \tag{3.6}$$

with  $A_0(0) + A_d(0) = 0$ . The spawn daughter singularity  $\zeta_d(t)$  moves according to the equation

$$\dot{\zeta}_d(t) = -q_{10}(\zeta_d(t), t) \quad \text{with } \zeta_d(0) = \zeta_0(0), \tag{3.7}$$

whereas the motion of the zero  $\zeta_0(t)$  is governed by

$$\dot{\zeta}_0(t) = -q_{10}(\zeta_0(t), t) - q_{20\zeta}(\zeta_0(t), t)[z_{\zeta\zeta}(\zeta_0(t), t)]^{-1}. \tag{3.8}$$

Thus,  $\zeta_0(t)$  and  $\zeta_d(t)$  travel at very different speeds. Depending on the initial data,  $\zeta_d(t)$  could have an impact on the interface when the zero is still far from the unit disk. For future reference, we define  $t_d$  to be the time at which the solution to (3.7) reaches the unit disk. For the data we consider here, equations (2.11)–(2.13) with  $A_0(0) = 1$  and  $\zeta_0(0) = 1.2$ ,  $t_d = 0.0463$ . Further inner asymptotic analysis of Tanveer (1993) suggests that the initial singularity  $\zeta_d(0)$  is transformed by the presence of surface tension into a cluster of an infinite number of  $-4/3$  singularities. The cluster is localized around  $\zeta_d(t)$  before it breaks up and disperse near the unit disk. Although the daughter singularity  $\zeta_d(t)$  reaches the unit disk in finite time, the asymptotic theory suggests that the actual  $-4/3$  singularities can get very close to the unit disk but do not hit it.

#### 4. An effective numerical method to study the limit

##### 4.1. Noise and the parametrization of the solution

All numerical quantities are affected by the presence of round-off noise whose magnitude is determined by the numerical precision. For example, the numerical solution of the interface position  $z_j(t)$  is perturbed by round-off errors  $\epsilon_j(t)$  in the form  $z_j(t) + \epsilon_j(t)$ . Let  $\hat{f}_k$  denote the  $k$ th mode of the discrete Fourier transform of  $f$ . From linear stability analysis around equilibrium, the Fourier modes of the noise  $\epsilon_j$  are subject to exponential growth

$$\hat{\epsilon}_k(t) = e^{\rho(k)t} \hat{\epsilon}_k(0),$$

where  $\rho(k) \approx |k| - B|k|^3$ . For sufficiently small  $B$ , many high modes grow very fast and the numerical solution  $z_j$  becomes severely polluted when  $|\hat{\epsilon}_k| > |\hat{z}_k|$ , i.e. when the noise dominates the physical solution.

Numerical filtering is an important tool to limit this spurious growth of noise. In particular, the nonlinear filter introduced by Krasny (1986) has proven to be very

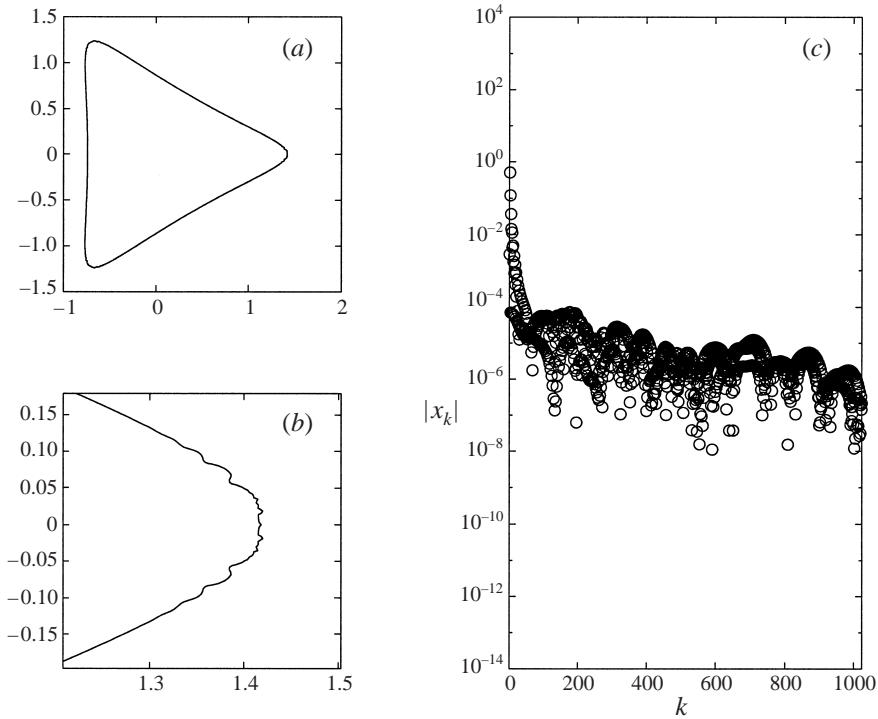


FIGURE 2. Helix-Shaw bubble at  $t = 0.054$  corresponding to  $\zeta_0 = 1.2$  and  $B = 10^{-6}$ . Computation performed in double precision using the equal-arclength parametrization. (a) The interface. (b) Close-up near one tip. (c) The Fourier spectrum of  $x$ .

successful in the computation of many ill-posed and nearly ill-posed problems. The Krasny filter is defined as follows. Given an error tolerance (filter level)  $\tau$ , the filter sets to zero all Fourier modes below this value, i.e.

$$\hat{f}^p_k = \begin{cases} \hat{f}_k & \text{if } |\hat{f}_k| > \tau \\ 0 & \text{if } |\hat{f}_k| \leq \tau. \end{cases}$$

It is important to note that this numerical filtering becomes ineffective for those modes above the filter level. Moreover, the filter truncates the natural decay of the Fourier coefficients and may very well suppress crucial information from the numerical solution. Indeed, the filter level establishes the effective precision for the numerical computations, and as such, it should be considered an important numerical parameter (see e.g. Shelley 1992). This issue is often overlooked.

The presence of surface tension implies additional numerical difficulties. Due to the high-order spatial derivatives introduced by the surface-tension term, explicit time integration methods have a severe stability constraint. A natural choice to handle this numerical stiffness is the boundary integral method designed by Hou, Lowengrub & Shelley (1994). This method is based on an equal-arclength parametrization of the interface and a small-scale decomposition of the interface evolution equations. These two components allow an efficient implementation of semi-implicit time discretizations that remove the high-order stability constraint. However, the equal-arclength frame which keeps the fluid particles uniformly distributed along the interface tends to introduce many significant high modes, above the filter level, in the numerical solution.



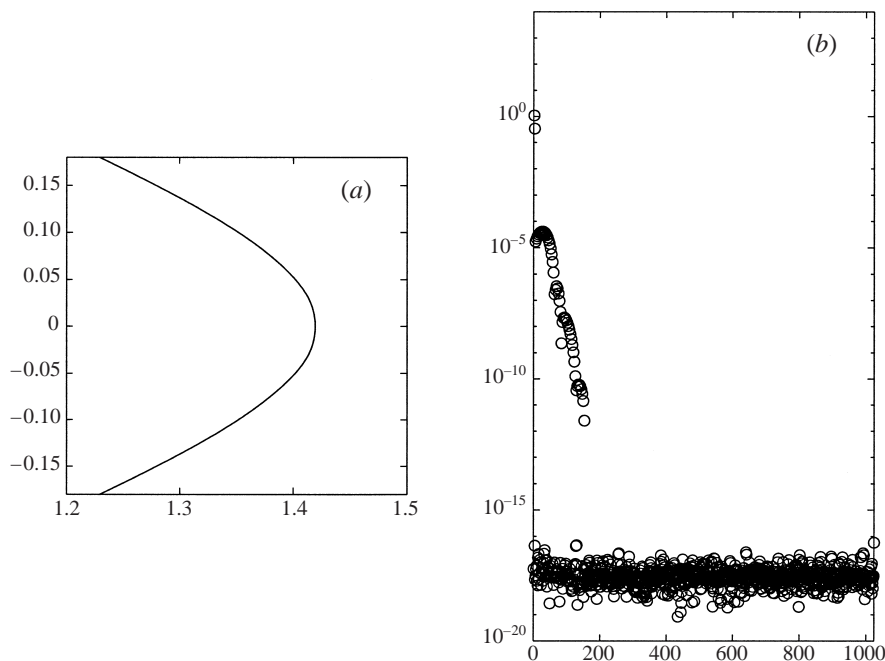


FIGURE 3. Hele-Shaw bubble at  $t = 0.054$  corresponding to  $\zeta_0 = 1.2$  and  $B = 10^{-6}$ . Computation performed in double precision using the conformal map parametrization. (a) Close-up of the interface near one tip. (b) The Fourier spectrum of  $x$ .

When surface tension is small, the round-off errors for these high-frequency modes have a large growth and the noise quickly dominates the numerical solution. This is illustrated in figure 2 which shows the interface and the spectrum of  $x$  computed with double precision (16 digits) using the equal-arclength parametrization. The solution is clearly polluted by noise as observed in both the interface and the spectrum of  $x$ . Note also that all the modes in the spectrum are well above round-off level ( $O(10^{-16})$ ) and thus cannot be filtered without seriously affecting the accuracy of the numerical solution.

Out of many choices (Lagrangian, equal-arclength, etc.), the parametrization provided by the conformal map description of the Hele-Shaw interface yields the most compact representation of the solution in Fourier space. This was first observed by Dai & Shelley (1993). The conformal parametrization was also employed by Siegel *et al.* (1996) for its especial compact representation property. In fact, for  $B = 0$ , the solution (2.11) has only two non-zero Fourier modes. High modes are introduced weakly through surface tension. Figure 3 shows the interface and the spectrum of the solution for  $B = 10^{-6}$ , computed using the conformal map frame and the same numerical parameters used for the previous equal-arclength computation. The spectrum of the solution is very clean and has only a few non-zero modes.

With this parametrization, we can use Krasny filtering effectively to separate noise from the physical solution for the majority of high to intermediate modes. Moreover, based on the symmetry of the solution, the Fourier expansion of  $z_\zeta(\zeta, t)$  for  $\zeta = e^{i\alpha}$  is given by

$$z_\zeta(\zeta, t) = \sum_{k=0}^{\infty} a_k(t) \zeta^{3k}, \quad (4.1)$$

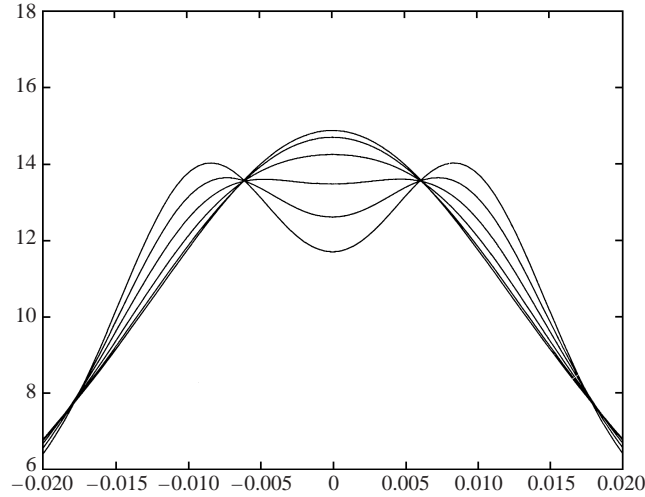


FIGURE 4. Tip curvature versus  $\alpha/2\pi$  at  $t = 0.054$ , computed with the conformal map frame in double precision and without scaling. At the centre, from top to bottom, the plots correspond to  $B = 0, 10^{-7}, 2.5 \times 10^{-7}, 5 \times 10^{-7}, 7.5 \times 10^{-7},$  and  $10^{-6}$ .

where the  $a_k$  are the Fourier coefficients of  $z_\zeta$  computed on the unit circle (see e.g. Dai *et al.* 1991). Thus, additional filtering in Fourier space can be performed to enforce (4.1), by setting to zero all the modes of  $z_\zeta$  that are not a multiple of 3.

In view of the previous remarks, the conformal map would seem to be the appropriate method to compute the zero-surface-tension limit. However, if we continue to decrease  $B$  further, we obtain a perfectly regular limit! This is illustrated in figure 4, where we show the curvature near one tip of the Hele-Shaw interface for different surface tensions decreasing from  $10^{-6}$  to  $10^{-7}$ , at  $t = 0.054$  (past  $t_d = 0.0463$ ). The corresponding curvatures approach the zero-surface-tension curvature. As we will see in the next section, this is an incorrect conclusion. For sufficiently small  $B$ , the method fails to capture the presence of the complex daughter singularity.

#### 4.2. Resolving extremely small $B$ : scaling and high precision

Recall that the daughter singularity is created at  $t = 0+$  in the complex  $\zeta$ -plane outside the unit disk. Initially, it is a very weak singularity. For times of  $O(\Delta t)$ , where  $\Delta t$  is the time step, the amplitude of the daughter singularity is  $O(B\Delta t)$ . Since the interface is analytic, its Fourier modes decay exponentially. As a result, many digits are required to capture the presence of the singularity in the complex plane.

Increasing the number of digits alone, i.e. computing in higher precision arithmetic, does not solve the problem as we are interested in the limiting behaviour of the interface as  $B$  tends to zero. To resolve the initially very weak singular contributions of surface tension for extremely small values of  $B$ , we combine high precision with a scaling of the interface evolution equation.

Given a non-zero surface tension solution  $Z$ , we are interested in the deviation of this solution from the zero-surface-tension solution  $Z_0$ . We can derive an equation for the scaled difference  $(Z - Z_0)/B$  by first noting that  $Z_0$  satisfies the equation  $Z_{0t} = F(Z_{0x})$ . Subtracting this equation from (2.6) and setting  $Z = Z_0 + B\tilde{Z}$  we get

$$\tilde{Z}_t = \frac{1}{B} [F(Z_{0x} + B\tilde{Z}_x) - F(Z_{0x})] + G(Z_{0x} + B\tilde{Z}_x). \quad (4.2)$$

The advantage of using this *scaled equation* is that the surface-tension term  $G$  is  $O(1)$  initially, independent of  $B$ . The term  $G$  contains the critical information about the complex singularity. The first term on the right-hand side of equation (4.2) is zero initially. Its contributions for short times are small compared to those coming from the surface-tension term. We propose here two different ways to evaluate this first term to avoid possible numerical instability caused by the division by  $B$ . One straightforward approach is to filter  $F(Z_{0x} + B\tilde{Z}_x) - F(Z_{0x})$  before dividing by  $B$ , and then filter the term obtained after the division. The disadvantage of this direct approach is that several digits are lost by the filtering process. A more stable evaluation is obtained by rewriting  $[F(Z_{0x} + B\tilde{Z}_x) - F(Z_{0x})]/B$  to factor  $B$  out. Note that

$$\frac{1}{B} [F(Z_{0x} + B\tilde{Z}_x) - F(Z_{0x})] = \int_0^1 \frac{1}{B} \frac{d}{ds} F(Z_{0x} + sB\tilde{Z}_x) ds. \tag{4.3}$$

Then, using (2.7) we have that

$$\begin{aligned} \frac{1}{B} \frac{d}{ds} F(Z_{0x} + sB\tilde{Z}_x) &= 2i(Z_{0x} + sB\tilde{Z}_x)(I - iH)|Z_{0x} + sB\tilde{Z}_x|^{-4} \\ &\quad \times \text{Re} \{ \tilde{Z}_x^*(Z_{0x} + sB\tilde{Z}_x) \} - i\tilde{Z}_x(I - iH)|Z_{0x} + sB\tilde{Z}_x|^{-2}, \end{aligned} \tag{4.4}$$

where the asterisk denotes complex conjugate. The leading factor  $B$  has been cancelled on the right-hand side of equation (4.4). This expression, which is a smooth function of the parameter  $s$ , can now be used to obtain a numerically stable evaluation of  $[F(Z_{0x} + B\tilde{Z}_x) - F(Z_{0x})]/B$  by performing the integral in (4.3) with relatively few points.

During the review of this paper, one of the referees pointed out an elegant and efficient way to scale the factor  $B$  in the left-hand side of (4.3) without having to evaluate the right-hand side integral. This efficient scaling can be obtained by separating the zero-surface-tension solution in the following form:

$$\frac{1}{|Z_x|^2} = \frac{1}{|Z_{0x}|^2} + Bh(\alpha), \tag{4.5}$$

where

$$h(\alpha) = \frac{-2\text{Re}(\tilde{Z}_x/Z_{0x}) - B|\tilde{Z}_x/Z_{0x}|^2}{|Z_x|^2} \tag{4.6}$$

and  $Z = Z_0 + B\tilde{Z}$ . Thus, from (2.7) we have that

$$F(Z_x) - F(Z_{0x}) = -BiZ_x(I - iH)h(\alpha) - Bi\tilde{Z}_x(I - iH)|Z_{0x}|^{-2}. \tag{4.7}$$

The right-hand side of this equation can be divided safely by  $B$  and the result can be evaluated with spectral accuracy using the fast Fourier transform (FFT).

The second important ingredient in capturing enough surface tension modes is to use very *high precision arithmetic* to solve numerically the scaled equation (4.2). High precision has the additional benefit of reducing the amplitude of the round-off noise. Variable high precision (up to 80 digits) was accomplished in this work with the use of the multi-precision package developed by Bailey (1990).

### 4.3. Highly accurate space–time discretization

We use a spectrally accurate spatial discretization of equation (4.2). All derivatives of  $\tilde{Z}$  and Hilbert transforms are computed using the discrete Fourier transform. The integral in (4.3) is approximated with a sixth-order Newton–Cotes quadrature formula and the result is compared with the direct approach explained above. The derivatives

of the exact zero-surface-tension solution  $Z_0$  are obtained analytically. Finally, the time integration is performed with a fourth-order explicit Adams–Bashforth method. Although implicit schemes give a less restrictive stability constraint than that of explicit methods, we do not benefit from their use here, as we are interested in the limiting behaviour as  $B \rightarrow 0$ . For the set of values of  $B$  we consider, the choice of  $\Delta t$ , as dictated by accuracy, turns out to be smaller than that imposed by the stability constraint. An implicit method would only be more efficient for much larger values of  $B$  than those considered here.

## 5. Numerical results

Since  $\tilde{Z} = (Z - Z_0)/B$ , where  $Z_0$  is the exact zero-surface-tension solution given by equation (2.11),  $\tilde{Z}$  is zero initially. Here, we take  $\zeta_0 = 1.2$  and  $A(0) = 1$  for which the daughter singularity time  $t_d = 0.0463$ , and the zero-surface-tension cusp singularities occur at  $t_c = 0.3301$  (see Siegel *et al.* 1996).

Our numerical experiments are divided in three parts. First, we compute the interface evolution for different decreasing values of  $B$  up to the time  $t = 0.048$ , which is slightly past  $t_d$ . These computations demonstrate the singular limiting behaviour of the interface. In the second part, we present more detailed information on the time and length scales near  $t_d$ , as  $B$  decreases. These numerical results provide further understanding of the surface-tension singular effects and are relevant to some of the scalings predicted by the asymptotic theory. Finally, we examine the impact of the daughter singularity by computing the evolution of the interface for a very small surface tension coefficient,  $B = 10^{-8}$ . The computations proceed up to the time where the effects of the complex singularity begin to be visible on the interface. The effects are compared with those produced by much large surface tensions.

Capturing the complex singularity also requires accurate time stepping. For each value of  $B$  and fixed spatial resolution, we successively halved the time step  $\Delta t$  until no difference (within plotting resolution in both the physical solution and the spectrum) was detected. It should be noted that  $\Delta t$  cannot be reduced arbitrarily. The product  $B\Delta t$  has to be well above the filter level so that enough Fourier modes of the daughter singularity are captured initially. Otherwise, for a given filter level, it is possible to choose  $\Delta t$  sufficiently small so that the daughter singularity would be completely filtered out. We also found that while the stability constraint for the explicit time integration is relaxed as the surface tension coefficient  $B$  decreases, the accurate computation of the singularity motion requires decreasing  $\Delta t$  linearly as  $B$  is reduced.

The computations started with  $N = 4096$  ( $N$  is the number of points along the whole interface).  $N$  was doubled to 8196 when the magnitude of the highest Fourier mode exceeded the filter level. The time step was then reduced by a factor of 8. The precision level was varied to verify that the complex singularity was well captured. We started with 40 digits of precision and compared with the solutions obtained with 60 digits. We observed an appreciable difference in the 40- and 60-digit solutions, particularly for the smallest values of  $B$  ( $10^{-8}$  and  $10^{-9}$ ). We increased the precision to 80 digits and found agreement with the 60-digit computations for all the values of  $B$  we considered here.

The use of variable high precision not only allowed us to ensure that the complex singularity was well captured but also provided a test for the presence of noise. The agreement of the solutions computed with extremely low filter levels,  $10^{-56}$  and  $10^{-78}$ , showed that noise effects were effectively controlled up to times slightly past  $t_d$ .

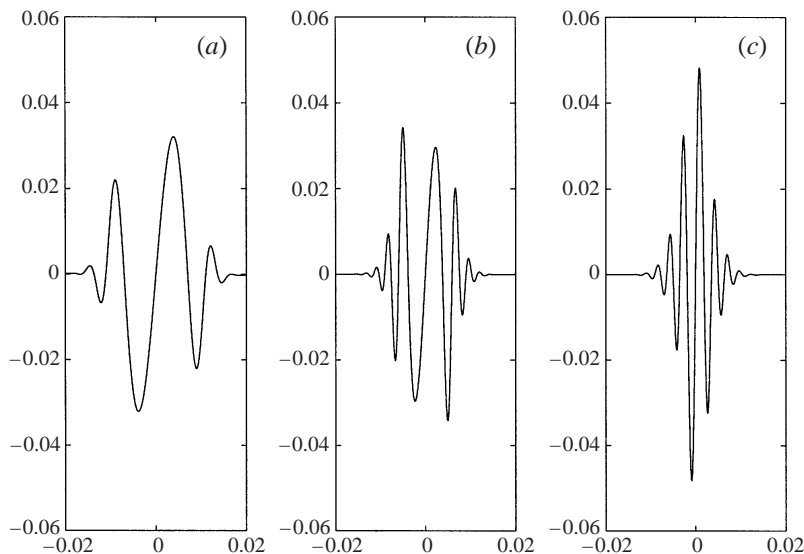


FIGURE 5.  $Z_\alpha - Z_{0\alpha}$  vs.  $\alpha/2\pi$  around one tip of the interface at  $t = 0.048$  for (a)  $B = 10^{-7}$ , (b)  $10^{-8}$ , and (c)  $10^{-9}$ .  $N = 8192$ . Precision level 60. Filter level  $10^{-56}$ .

As explained in § 4.2, we compute the term  $[F(Z_{0\alpha} + B\tilde{Z}_\alpha) - F(Z_{0\alpha})]/B$  in two different ways. The evaluation of this term using the integral in (4.3) is performed with a sixth-order Newton–Cotes formula with  $M$  points. Since the integrand is a smooth function of the parameter  $s$ , very few points are actually needed for an accurate evaluation. By varying  $M$  and comparing with the direct evaluation, we found that the integral is well-resolved for  $M = 32$ . On the other hand, the direct evaluation requires higher precision to compensate for the digits lost in the filtering process. For the range of  $B$  values we considered, the direct evaluation is computationally faster than performing the integral. However, for much smaller  $B$ , the evaluation through the integral would be both more stable and faster as the overhead for the higher precision needed for the direct evaluation would be significant.

### 5.1. The singular limiting behaviour

We present in this part computations performed for  $B = 10^{-7}$ ,  $10^{-8}$ , and  $10^{-9}$ . Figure 5 shows  $Z_\alpha - Z_{0\alpha}$  plotted against  $\alpha/2\pi$  around one tip of the interface and at the fixed time  $t = 0.048$ . Note that this time is already past  $t_d$ . As  $B$  decreases from  $10^{-7}$  to  $10^{-9}$ ,  $\max_\alpha |Z_\alpha - Z_{0\alpha}|$  does not decrease. In fact, it has a moderate growth. This is a clear indication of the singular limiting behaviour. A shrinkage of the length scale is also observed in figure 5. The distance between the two maxima of  $|Z_\alpha - Z_{0\alpha}|$  decreases as  $B$  is reduced. We give more details about the length scale in § 5.2.

The singular nature of the asymptotic solution is better appreciated in the deviations of the  $B > 0$  curvatures from the corresponding zero-surface-tension curvature. As observed in figure 6, the deviations are significant and rather localized at the fixed time  $t = 0.048$ . Indeed, the smaller the surface tension the larger the deviation.

At  $t = 0.048$ , the surface-tension effects are still inappreciable at the interface itself. As figure 7 shows, the derivative of the curvature  $\mathcal{K}_\alpha$  is very large at this time (about  $3 \times 10^4$  for  $B = 10^{-9}$ ) but the surface-tension term  $B\mathcal{K}_\alpha$  is still very small at  $t = 0.048$ , for the values of  $B$  considered. Note that  $t = 0.048$  is only slightly past  $t_d$ . According to Siegel *et al.* (1996), the surface-tension term becomes  $O(1)$  when  $t = t_d + O(1)$ ,

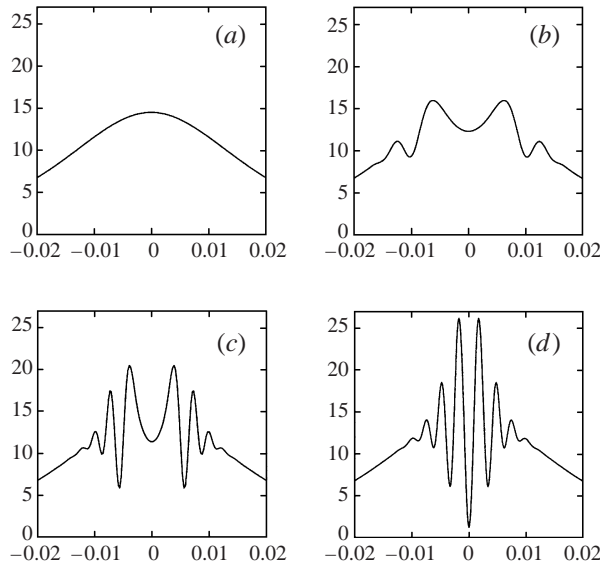


FIGURE 6. Curvature vs.  $\alpha/2\pi$  around one tip of the interface at  $t = 0.048$  for (a)  $B = 0$ , (b)  $10^{-7}$ , (c)  $10^{-8}$ , and (d)  $10^{-9}$ .  $N = 8192$ . Precision level 60. Filter level  $10^{-56}$ .

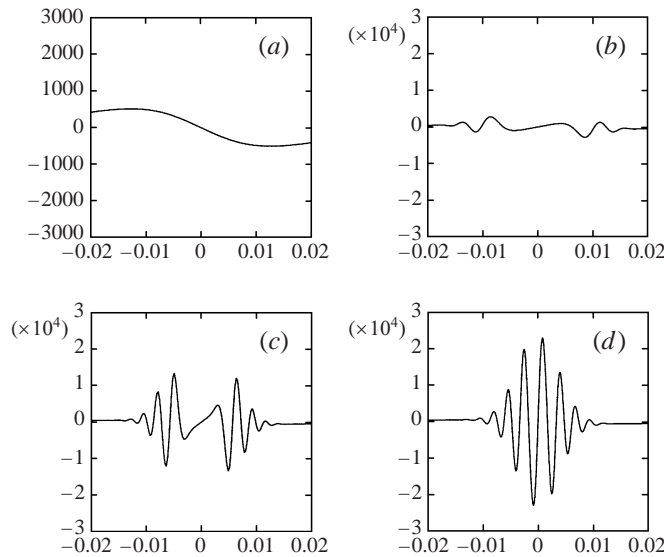


FIGURE 7.  $\mathcal{K}_\alpha$  vs.  $\alpha/2\pi$  around one tip of the interface at  $t = 0.048$  for (a)  $B = 0$ , (b)  $10^{-7}$ , (c)  $10^{-8}$ , and (d)  $10^{-9}$ .  $N = 8192$ . Precision level 60. Filter level  $10^{-56}$ . Note the different scale used for  $B = 0$ .

regardless of the value of  $B$ . This is when the  $B > 0$  interface has an  $O(1)$  deviation from the  $B = 0$  solution.

Another clear sign of the singular limiting behaviour is given in figure 8. The spectrum of  $\tilde{X} = \text{Re}\{\tilde{Z}\}$  is plotted for  $B = 10^{-7}$ , and  $B = 10^{-8}$  before and after  $t_d$ . For early times both spectra almost coincide then, as  $t_d$  is approached, they rise and separate. The spectrum corresponding to  $B = 10^{-8}$  rises higher indicating a more singular solution.

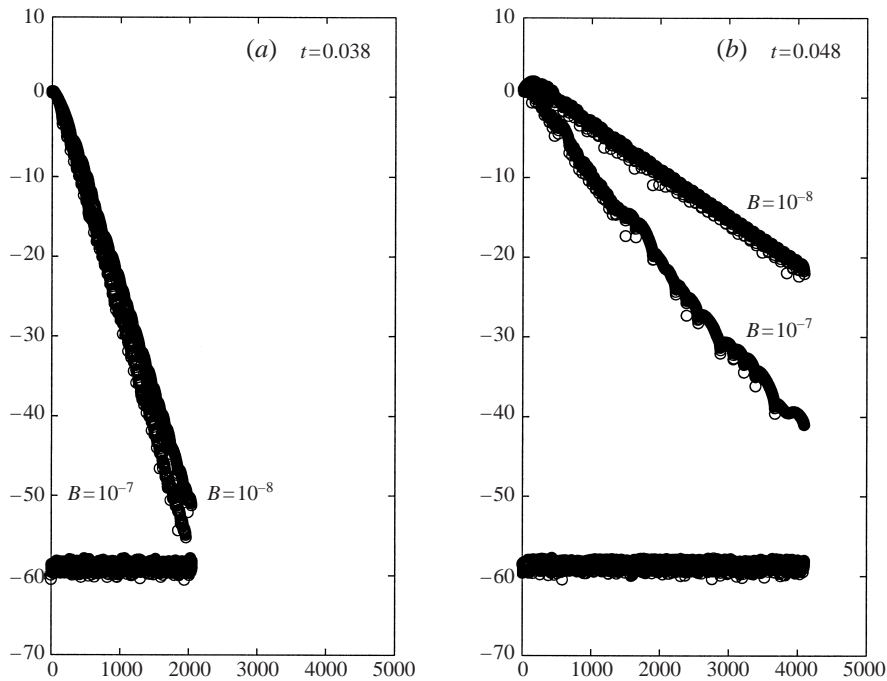


FIGURE 8. The spectrum of  $\tilde{X}$  for  $B = 10^{-7}$  and  $B = 10^{-8}$ , before (a) and after (b)  $t_d$ .

5.2. Time and space scalings near  $t_d$

The quantification of the deviations of the  $B > 0$  solutions from the  $B = 0$  solution, and the time (as defined below) when these deviations first occur, provide very important information. In the limit as  $B \rightarrow 0$ , this information can be related to the size and the motion of the complex singularity cluster as it approaches the physical domain. It also gives a comparison point for some of the scalings predicted by the asymptotic theory.

Following Siegel *et al.* (1996), we define  $t_q$  as the first time at which  $\max |Z_\alpha(\alpha, t) - Z_{0\alpha}(\alpha, t)| = q$ . Given that the daughter singularity is actually a cluster of singularities,  $t_q$  as a function of  $B$  gives useful information about the size of the cluster as it approaches the unit disk. According to the asymptotic theory, the size of the singularity cluster is  $O(B^{1/3})$ . The effects of the daughter singularity will be felt when the leading edge of the cluster reaches the unit disk. Therefore,  $t_q$  should vary linearly with  $B^{1/3}$ , for sufficiently small  $q$  and  $B$ . Figure 9 shows log-log plots of  $t_d - t_q$  for a set of values of  $B$ , and  $q = 0.0001, 0.0002$ , and  $0.0005$ . We computed the slopes obtained from every two adjacent points in the curves and took the average. The average slopes are: 0.3819, 0.3969, and 0.4150 respectively. While slightly above  $1/3$ , the slopes tend to decrease as  $q$  is reduced. The values of the slopes are similar to those reported by Siegel *et al.* (1996).

Information about the size of the singularity cluster can also be obtained by measuring the length of the region most affected by surface tension. More precisely, we define the length  $s_p(t)$  to be twice the largest  $\alpha \in [0, \pi/3]$  for which  $|Z_\alpha(\alpha, t) - Z_{0\alpha}(\alpha, t)| > p$ . The asymptotic theory suggests that, when the daughter singularity is in the proximity of the unit disk, the appropriate time variable should

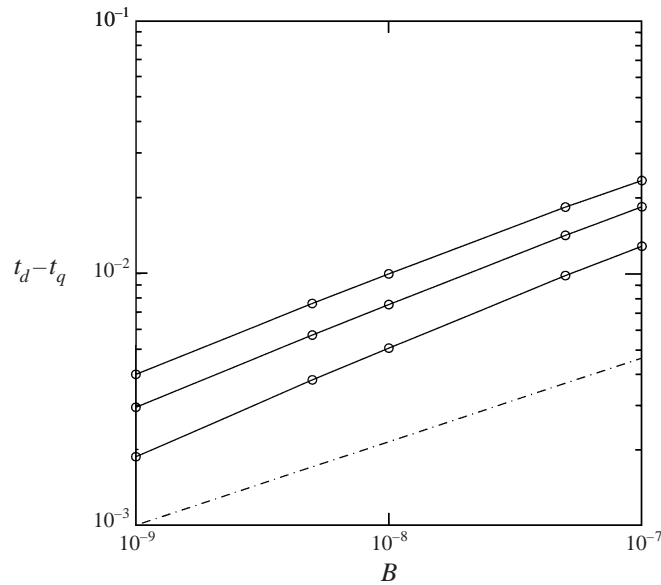


FIGURE 9. Log-log plot of  $t_d - t_q$  versus  $B$ . From top to bottom, the solid curves correspond to  $q = 0.0001, 0.0002,$  and  $0.0005$ . The average slopes are  $0.3819, 0.3969,$  and  $0.4150$  respectively. The dot-dashed line is the  $1/3$ -slope line predicted by the asymptotic theory.

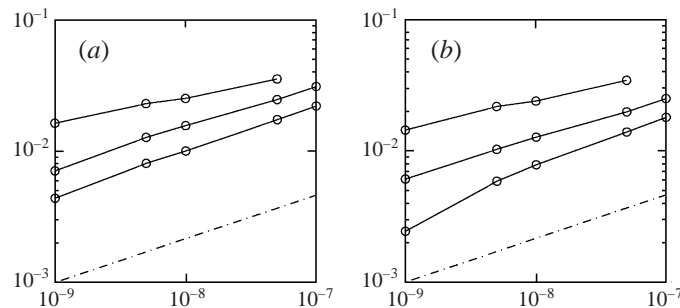


FIGURE 10. Log-log plot of  $s_p$  versus  $B$ . From top to bottom the solid curves correspond to the scaled time  $T = 1, T = 0,$  and  $T = -1$ . The dot-dashed line is the  $1/3$ -slope line predicted by the asymptotic theory. (a)  $p = 0.0005$ ; (b)  $p = 0.001$ .

be defined as (see Siegel *et al.* 1996, §4.2)

$$T = \frac{t - t_d}{B^{1/3}}. \quad (5.1)$$

In figure 10, we plotted  $s_p$  at the scaled times  $T = -1, 0$  ( $t = t_d$ ), and  $1$ . The curves corresponding to  $T = -1$  and  $T = 0$ , for the smallest value of  $p$  (figure 10a), have an average slope very close to  $1/3$ . This is in agreement with the asymptotic theory. Although the curves corresponding to  $T = 1$  do not show a clear linear behaviour, it is observed that their average slopes are much less than  $1/3$ , suggesting that the singularity cluster gets squeezed after  $t_d$ . However, this result is not conclusive. The solutions at  $T = 1$  are more difficult to resolve and the unevenness of the  $T = 1$  curve may be due to insufficient resolution for some of the values of  $B$  considered.

We have also measured the maximum value of the surface-tension term  $B\mathcal{H}_\alpha$  at



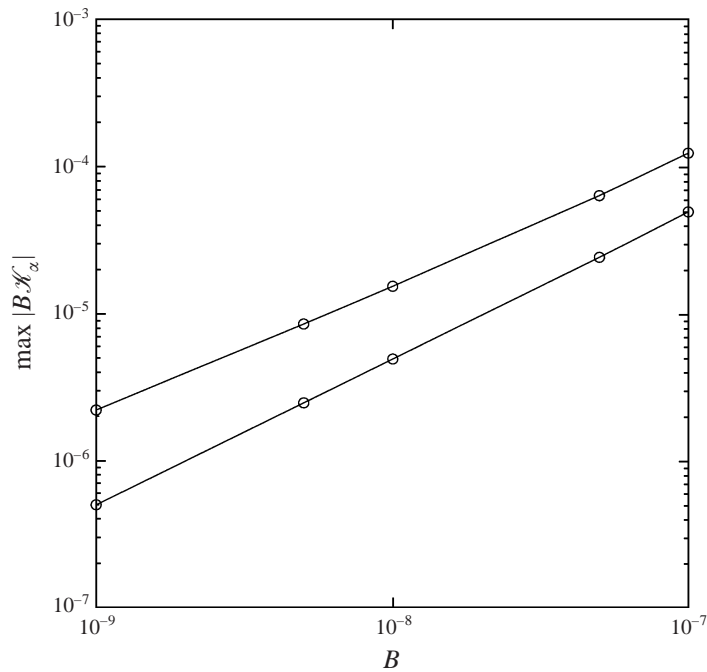


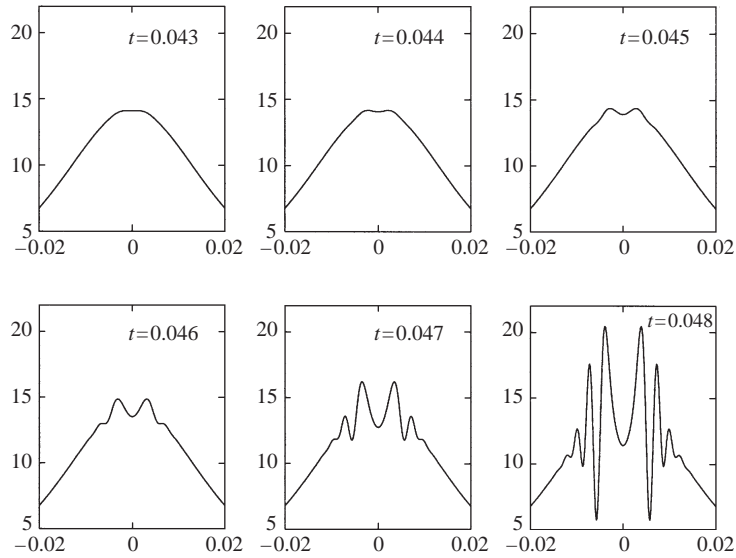
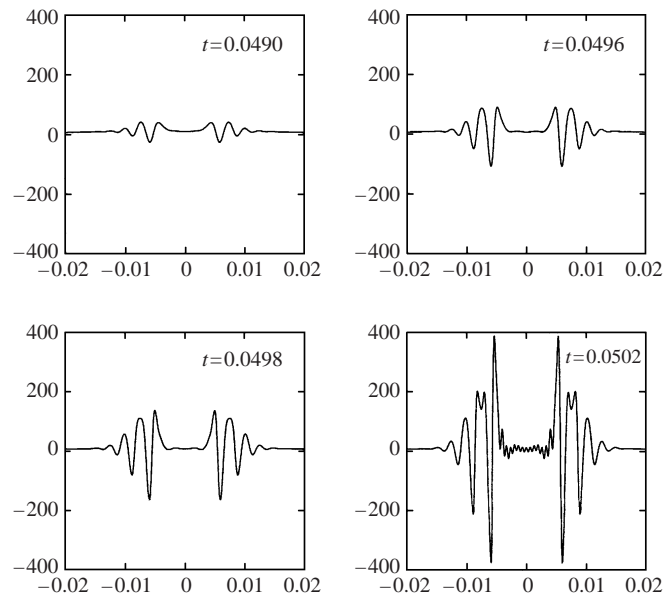
FIGURE 11. Log-log plot of  $\max |B\mathcal{K}_\alpha|$  versus  $B$ . The top curve corresponds to  $T = 0$  (average slope is 0.8556) and bottom one to  $T = -1$  (average slope is 0.9963). The slope predicted by the asymptotic theory is  $1/3$ .

the scaled times  $T = -1$  and  $T = 0$ . The two corresponding curves of  $\max |B\mathcal{K}_\alpha|$  appear in figure 11. For the earlier time  $T = -1$ , there is a clear linear behaviour with an average slope very close to 1. On the other hand, at  $T = 0$  ( $t = t_d$ ), the behaviour is uneven but with a smaller average slope (0.8856). For the three smallest values of  $B$  computed, the average slope is 0.8489. This small slope, less than 1, is another indication of the singular limit. As  $B \rightarrow 0$ ,  $|\mathcal{K}_\alpha|$  would diverge at  $t_d$ . The slope predicted by the asymptotic theory is  $1/3$ .

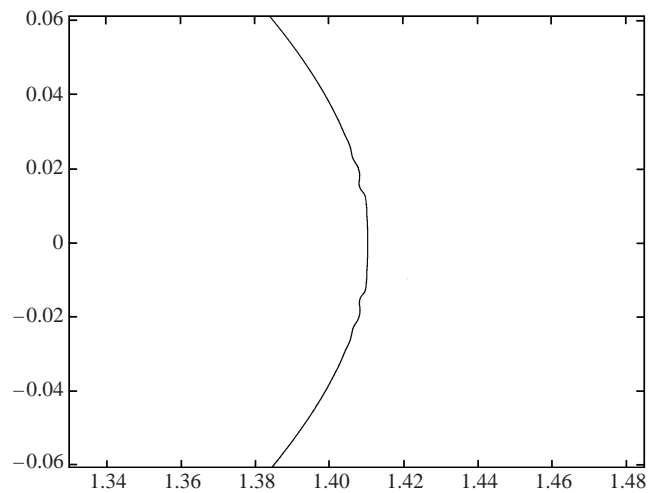
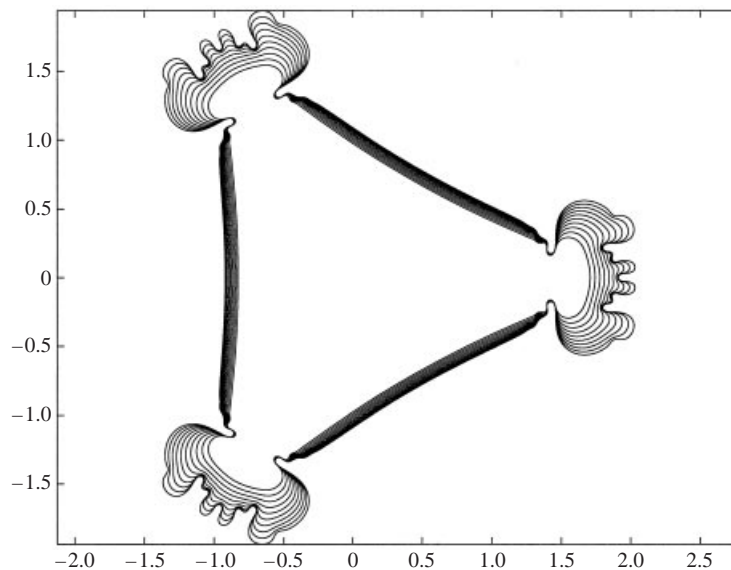
### 5.3. The impact of the daughter singularity

We present first a sequence of pictures of the interface curvature near one tip at early times near  $t_d$  (figure 12). The computations correspond to  $B = 10^{-8}$ . The proximity of the daughter singularity to the physical domain is already felt at the time  $t = 0.043$  around the interface tips. At  $t = 0.043$ , the tip curvature flattens in a very localized finite region. This is in agreement with the theoretical small but non-zero size of the compact singularity cluster. The curvature subsequently develops large deviations from the zero-surface-tension curvature and the affected regions near three tips spread in time. This behaviour is consistent with the asymptotic theory that predicts that the daughter singularity cluster will disperse once it gets very close to the unit disk. Note also that the number of local maxima in the curvature is growing in time. It is conceivable that, as suggested by Siegel *et al.* (1996), the singularity cluster breaks up after  $t_d$  into subclusters that spread around the physical domain.

A longer-time computation identifies the impact of the daughter singularity on the interface. The computation was performed up to  $t_d$  using 60-digit arithmetic. Shortly after that, we switched to double precision when the highest mode of  $\tilde{Z}$  was

FIGURE 12. Tip curvature for  $B = 10^{-8}$  at early times near  $t_d = 0.0463$ .FIGURE 13. Curvature near tip for  $B = 10^{-8}$  at different times after  $t_d$ .  $N = 8192, 16384,$  and  $32768$  (double precision).

about  $10^{-15}$ . The number of points was doubled (and  $\Delta t$  was reduced by a factor of 8) whenever the spectrum became under-resolved. We stop the computation with  $N = 32768$  and  $\Delta t = 10^{-7}$ . The curvature of the solution at subsequent times is presented in figure 13. In a very short time interval, the maximum of curvature has grown by more than 10 times its value at  $t = 0.049$ , and the singular regions (near the three tips of the interface) continue to spread in time. Despite the complicated structure, the two innermost symmetric maxima in the curvature define a clear length scale. At  $t = 0.0502$ , very small oscillations around  $\alpha = 0$  are observed in the curvature.

FIGURE 14. Close-up of the interface at  $t = 0.0502$  for  $B = 10^{-8}$ .FIGURE 15. Evolution of the Hele-Shaw interface for  $B = 10^{-4}$ . The interface profiles correspond to the times  $t = 0.23$ – $0.50$ , with a  $0.03$  time difference between profiles. Computation performed with the equal-arclength method.

It is possible that these oscillations are caused by noise which is affecting many more high-frequency components at this stage. Nevertheless, the largest minimum-to-maximum transition dominates the effects observed in the actual interface. Indeed, as figure 14 shows, the singular effects are already visible in the interface. The small indentations near the interface tip correspond to the largest curvature transition. These side indentations are a signature of surface tension.

For larger  $B$ , the indentations appear farther off the centre of the interface tip (see Dai *et al.* 1991; Siegel *et al.* 1996). We illustrate this with a pair of computations performed using the equal-arclength method of Hou *et al.* (1994). Our method

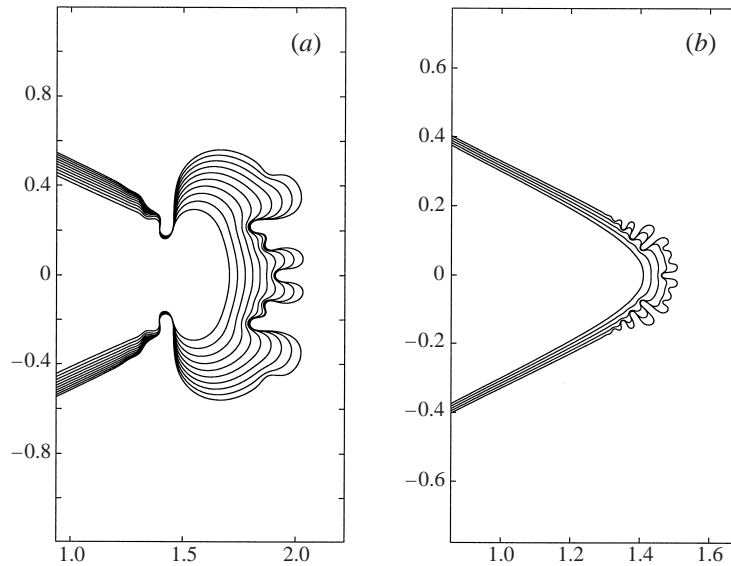


FIGURE 16. Close-ups of the Hele-Shaw interface at different times for (a)  $B = 10^{-4}$  ( $t = 0.23$ – $0.50$ , with a 0.03 time difference between profiles) and (b)  $B = 10^{-5}$  ( $t = 0.05$ – $0.09$ , with a 0.01 time difference between profiles). Computation performed with the equal-arclength method.

presented here cannot compute accurately for larger surface tension due to time-stepping limitations. Figure 15 shows the evolution of the interface for  $B = 10^{-4}$ . The symmetric indentations are clearly formed before the noise-induced tip splitting occurs. Figure 16 gives a close-up of the interface near one tip at different times for  $B = 10^{-4}$  and  $B = 10^{-5}$ , both cases computed with the equal-arclength method. For  $B = 10^{-5}$ , the side indentations produced by surface tension begin to be visible in the second curve from the left. Shortly after that the tip-splitting process and the finger formation begin.

It is important to note the fast growth that the curvature and its derivative have shortly after  $t_d$ . This rapid growth is shown in figure 17 for  $B = 10^{-8}$ . The large and fast transition observed may give the impression of a finite-time curvature singularity. This seems to be unlikely in view of the long-time behaviour observed for larger  $B$ . The rescaling features of the asymptotic theory inner-scale equation (Siegel *et al.* 1996) suggest that, if solutions exist for larger  $B$ , they will exist for any non-zero  $B$ , at least well beyond  $t_d$ . In view of this, a more plausible scenario is the following. The daughter singularity cluster will asymptotically shrink to a point, in the limit as  $B$  is decreased. The compact cluster will get within a maximal distance of  $O(B^{1/2})$  to the unit disk but will not hit it in finite time. As explained below, this close proximity of the singularity cluster to the physical domain can cause a fast transition in the interface curvature. If the  $B > 0$  solutions exist for all times, surface tension will define a length scale according to the minimum distance of the complex singularity to the unit disk.

## 6. Conclusions

A numerical investigation of the singular effects of surface tension on an evolving Hele-Shaw interface has been presented. We designed an innovative numerical method

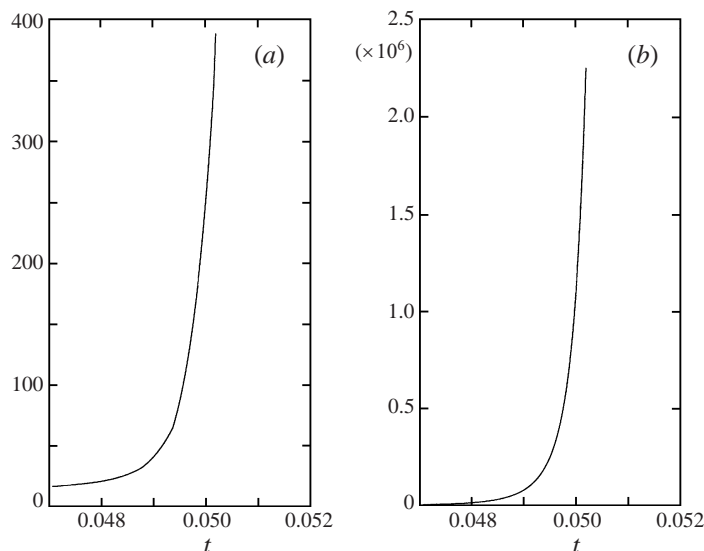


FIGURE 17. The maximum of  $|\mathcal{K}|$  vs. time (a) and the maximum of  $|\mathcal{K}_x|$  vs. time (b) for  $B = 10^{-8}$ .

to overcome the extreme noise sensitivity of the problem and to capture the surface-tension-induced complex singularity in the limit as the surface tension coefficient  $B$  tends to zero. By combining a compact parametrization of the interface, a scaling of the evolution equations, and very high precision, we obtain a numerical method that greatly reduces the effect of noise and allows us to identify the true effects of surface tension.

Through a series of intensive computations for extremely small values of the surface tension coefficient we demonstrated clearly that the limiting behaviour of the interface as  $B$  tends to zero is singular. The onset of the singular effects is well predicted by following the theoretical impact time of the daughter singularity cluster on the physical domain. Our numerical results reflect, in accordance with the asymptotic theory of Tanveer and of Siegel, Tanveer & Dai, that a surface-tension-induced (daughter) singularity can produce  $O(1)$  effects on the interface when the zero-surface-tension solution is still smooth. The singular effects are very localized and the size of the affected regions decreases as  $B$  is reduced. It is also found that, after the daughter singularity impact time and for a fixed surface tension, the singularly affected regions slowly spread in time. This behaviour supports the theory that the daughter singularity is a compact cluster of singularities that breaks up and spreads around the unit disk after the impact time (Siegel *et al.* 1996).

At a later stage of the motion it is observed that the interface curvature has a rapid and large growth in a short period of time around the localized singular regions. This rapid variation detected by the numerics can give the impression of a finite-time curvature singularity. However, the asymptotic theory suggests that the compact singularity cluster will get very close (within an  $O(B^{1/2})$  distance) to the unit disk but will not hit it in finite time. Since  $z_{\zeta\zeta}$  scales as  $B^{-1/3}$  in the inner region characterizing the daughter singularity cluster, the proximity of this cluster to the physical domain can cause the curvature to change from  $O(1)$  to  $O(B^{-1/3})$  over an  $O(B^{1/3})$  time scale. Thus, it is conceivable that the rapid transition in the curvature growth reflects this change of scales. Unfortunately, we cannot compute accurately much beyond the

stage of the rapid transition. Long-time computations are extremely difficult due to the spreading of Fourier modes and the impact of noise. Nevertheless, it is observed that surface tension defines a length scale for the subsequent finger formation and tip-splitting processes.

We would like to thank Saleh Tanveer and Mark Kunka for teaching us much about the daughter singularity and the asymptotic theory. We also benefitted greatly from the advice of Pingwen Zhang and Helen Si about the numerical aspects of this work. This research is supported in part by a ONR grant N00014-96-1-0438 and by a NSF grant DMS-9704976.

## REFERENCES

- ARNEODO, A., COUDER, Y., GRASSEU, G., HAKIM, V. & RABAU, M. 1989 Uncovering the analytical Saffman–Taylor finger in unstable viscous fingering and diffusion limited aggregation. *Phys. Rev. Lett.* **63**, 984–987.
- BAILEY, D. H. 1990 MPFUN: A portable high performance multiprecision package. *Tech. Rep.* RNR-90-022. NASA Ames Research Center.
- BENSIMON, D. 1986 Stability of viscous fingering. *Phys. Rev. A* **33**, 1302–1308.
- CONSTANTIN, P. & KADANOFF, L. 1991 Dynamics of a complex interface. *Physica D* **47**, 450–460.
- CONSTANTIN, P. & PUGH, M. 1993 Global solutions for small data to the Hele-Shaw problem. *Nonlinearity* **6**, 393–415.
- DAI, W.-S., KADANOFF, P. & ZHOU, S.-M. 1991 Interface dynamics and the motion of complex singularities. *Phys. Rev. A* **43**, 6672–6682.
- DAI, W.-S. & SHELLEY, M. J. 1993 A numerical study of the effect of surface tension and noise on an expanding Hele-Shaw bubble. *Phys. Fluids A* **5**, 2131–2146.
- DEGREGORIA, A. J. & SCHWARTZ, L. W. 1986 A boundary-integral method for two-phase displacement in Hele-Shaw cells. *J. Fluid Mech.* **164**, 383–400.
- DUCHON, J. & ROBERT, R. 1984 Évolution d’une interface par capillarité et diffusion de volume I. Existence locale en temps. *Ann. Inst. Henri Poincaré* **1**, 361–378.
- HOU, T. Y., LOWENGRUB, J. S. & SHELLEY, M. J. 1994 Removing the stiffness from interfacial flows with surface tension. *J. Comput. Phys.* **114**, 312–338.
- HOWISON, S. D. 1986a Bubble growth in porous media and Hele-Shaw cells. *Proc. R. Soc. Edinb. A* **102**, 141–148.
- HOWISON, S. D. 1986b Cusp development in Hele-Shaw flow with a free surface. *SIAM J. Appl. Maths* **46**, 20–26.
- HOWISON, S. D. 1986c Fingering in Hele-Shaw cells. *J. Fluid Mech.* **167**, 439–435.
- KRASNY, R. 1986 A study of singularity formation in a vortex sheet by the point vortex approximation. *J. Fluid Mech.* **167**, 65–93.
- MAXWORTHY, T. 1987 The nonlinear growth of a gravitationally unstable interface in a Hele-Shaw cell. *J. Fluid Mech.* **177**, 207–232.
- MEIBURG, E. & HOMS, G. M. 1988 Nonlinear unstable viscous fingers in Hele-Shaw flows. II. Numerical simulation. *Phys. Fluids* **31**, 429–439.
- PELÉ, P. 1988 *Dynamics of Curved Fronts*. Academic.
- SAFFMAN, P. G. 1959 Exact solutions for the growth of fingers from a flat interface between two fluids in a porous medium. *Q. J. Mech. Appl. Maths* **12**, 146–150.
- SHELLEY, M. J. 1992 A study of singularity formation in vortex sheet motion by a spectrally accurate vortex method. *J. Fluid Mech.* **244**, 493–526.
- SHRAIMAN, B. & BENSIMON, D. 1984 Singularities in nonlocal interface dynamics. *Phys. Rev. A* **30**, 2840–2842.
- SIEGEL, M., TANVEER, S. & DAI, W.-S. 1996 Singular effects of surface tension in evolving Hele-Shaw flows. *J. Fluid Mech.* **323**, 201–236.
- TANVEER, S. 1993 Evolution of Hele-Shaw interface for small surface tension. *Phil. Trans. R. Soc. Lond. A* **343**, 155–204.